ЖЭТФ, 2015, том 148, вып. 4 (10), стр. 766–777

KINEMATIC DUST VISCOSITY EFFECT ON LINEAR AND NONLINEAR DUST-ACOUSTIC WAVES IN SPACE DUSTY PLASMAS WITH NONTHERMAL IONS

A. M. El-Hanbaly [a], ***M. Sallah*** [a*], ***E. K. El-Shewy*** [b], ***H. F. Darweesh*** [a]

[a] *Physics Department, Faculty of Science, Mansoura University 35516, Mansoura, Egypt*

[b] *Department of Physics, Taibah University Al-Madinah Al-Munawarah, Saudi Arabia*

Received December 30, 2014

Linear and nonlinear dust-acoustic (DA) waves are studied in a collisionless, unmagnetized and dissipative dusty plasma consisting of negatively charged dust grains, Boltzmann-distributed electrons, and nonthermal ions. The normal mode analysis is used to obtain a linear dispersion relation illustrating the dependence of the wave damping rate on the carrier wave number, the dust viscosity coefficient, the ratio of the ion temperature to the electron temperatures, and the nonthermal parameter. The plasma system is analyzed nonlinearly via the reductive perturbation method that gives the KdV–Burgers equation. Some interesting physical solutions are obtained to study the nonlinear waves. These solutions are related to soliton, a combination between a shock and a soliton, and monotonic and oscillatory shock waves. Their behaviors are illustrated and shown graphically. The characteristics of the DA solitary and shock waves are significantly modified by the presence of nonthermal (fast) ions, the ratio of the ion temperature to the electron temperature, and the dust kinematic viscosity. The topology of the phase portrait and the potential diagram of the KdV–Burgers equation is illustrated, whose advantage is the ability to predict different classes of traveling wave solutions according to different phase orbits. The energy of the soliton wave and the electric field are calculated. The results in this paper can be generalized to analyze the nature of plasma waves in both space and laboratory plasma systems.

DOI: 10.7868/S0044451015100144

1. INTRODUCTION

There has been a great interest in the understanding of different types of collective processes in dusty plasmas, because of their vital role in the study of astrophysical and space environments, such as cometary tails, asteroid zones, planetary rings, the insterstellar medium, Earth's environment, etc. [1–4]. The dust grains are usually negatively charged because of a number of charging processes, such as field emission, ultraviolet radiation, plasma currents, etc. [5–7]. The presence of this charged dust component not only modifies the existing plasma wave spectra but also introduces new eigenmodes, such as the dust-acoustic (DA) mode [8, 9], dust–ion acoustic mode [10], dust cyclotron mode [11], dust drift mode [12], dust lattice mode [13, 14], etc. The DA wave is the most well studied of such new modes. It arises due to the restoring force provided by the plasma thermal pressure electrons and ions, while the inertia is due to the dust mass [8, 9].

In particular, the hot electrons may not follow the Maxwellian distribution. In [15], the effect of nonthermal electrons was proposed for observations by the Freja satellite. On the other hand, nonthermal (fast) ions have been observed in Earth's bow-shock [16]. The combined effects of the nonadiabatic dust charge fluctuation and the fast (nonthermal) ions on the propagation of linear DA waves in inhomogeneous dusty plasmas were studied in [17]. The presence of nonthermality of ions was shown to modify the frequency and damping of the low-frequency plasma mode. Therefore, it is reasonable to consider the nonthermality of plasma ions throughout this work.

*E-mail: msallahd@mans.edu.eg

It is important to investigate the nonlinear DA waves to understand the properties of localized electrostatic perturbations in space and laboratory dusty plasmas [1, 18–20]. Recently, the nonlinear DA waves have been investigated theoretically [8, 21–24] as well as experimentally [25, 26]. All of the theoretical and experimental investigations have been carried out at room temperature.

In most of the theoretical studies on dusty plasma, the reductive perturbation method has been used for deriving the Korteweg–de Vries (KdV), Korteweg–de Vries–Burgers (KdV–Burgers), Zakharov–Kuznetsov, and Kadomtsev–Petviashvili equations [27–29]. The reductive perturbation method is mostly applied to small-amplitude nonlinear waves [30]. This method rescales both space and time in the governing equations of the system in order to introduce space and time variables that are appropriate for the description of long-wavelength phenomena.

Moreover, dusty plasmas with dissipative characteristics support the existence of shock waves instead of soliton waves. The dissipation in dusty plasmas can be caused by the Landau damping, dust fluid viscosity, dust–dust collisions, and dust charge fluctuations, which could modify the wave properties [31, 32]. Experimentally, the effects of dissipation caused by the kinematic viscosity on the propagation of solitary wave structures are observed and discussed in [33]. The DA shock waves in dusty plasma with dust charge fluctuations and nonthermal ion effects were studied in [34] using the reductive perturbation technique to derive a KdV–Burgers equation. The effect of nonthermal ions was considered in [35] and the KdV equation was obtained; in [36], the same nonthermal plasma model was considered and the modified KdV equation was derived. The results in [35, 36] showed the solitary waves with finite amplitude only.

In this paper, we consider a homogeneous system of an unmagnetized, collisionless and dissipative dusty plasma that consists of negatively charged dust grains, Boltzmann-distributed electrons, and nonthermal (fast) ions (Sec. 2). The linear dispersion relation is analyzed by using the normal mode technique. It shows the dependence of the plasma damping rate on the different plasma parameters (Sec. 3). To emphasize the nonlinearity of the analysis, the reductive perturbation method is used, which yields a nonlinear partial differential equation, the KdV–Burgers equation (Sec. 4). Topologically, we illustrate the bifurcation and phase portrait of the KdV–Burgers equation in order to recognize the different classes of nonlinear waves.

2. GOVERNING EQUATIONS

We consider a homogeneous system of an unmagnetized, collisionless and dissipative dusty plasma whose constituents are negatively charged dust grains, nonthermal ions, and electrons obeying the Boltzmann thermal distribution. The dynamics of the DA waves are governed by the basic set of equations

$$\frac{\partial n_d}{\partial t} + \frac{\partial \left(n_d u_d\right)}{\partial x} = 0, \tag{1}$$

$$\frac{\partial u_d}{\partial t} + u_d \frac{\partial u_d}{\partial x} + q\frac{\partial \phi}{\partial x} - \eta_d \frac{\partial^2 u_d}{\partial x^2} = 0, \tag{2}$$

$$\frac{\partial^2 \phi}{\partial x^2} + q n_d - n_e + n_{_i} = 0, \tag{3}$$

where n_d is the dust grain number density, u_d is the dust fluid velocity, q is the number of charges on the dust grains, ϕ is the electrostatic potential, η_d is the dust viscosity coefficient, n_e is the electron number density and $n_{_i}$ is the ion number density.

As usual, the dust charge is a function of the plasma parameters, but as a consequence of that, the typical dust charging time scale may be longer than the DA time scale, and we anticipate that the dust charge fluctuations have no essential effect on the DA mode, and the dust charge can therefore be assumed to be constant [37, 38]. When the effects of plasma turbulence, particle reflection, Landau damping, and charge fluctuations are not significant, the kinematic dust viscosity provides an alternative physical mechanism that causes dissipation in a dusty plasma and leads normally to shock waves. Here, the kinematic dust viscosity is considered to be constant [39].

The thermal and nonthermal distributions of the electrons and ions are chosen to be

$$n_e = \mu_e \exp\left(\sigma_i \phi\right), \tag{4}$$

$$n_{_i} = \mu_i \left[1 + \beta\phi + \beta\phi^2\right] \exp\left(-\phi\right), \tag{5}$$

where μ_i and μ_e are the initial equilibrium density of ions and electrons, $\beta = 4\alpha/(1+3\alpha)$, α is a parameter determining the number of fast nonthermal ions, and $\sigma_i = T_i/T_e$, where T_e is the temperature of electrons and T_i is the temperature of ions.

3. LINEAR ANALYSIS

To derive a dynamical equation for the dispersion relation of DA waves from the basic equations (1)–(5),

we use the normal mode method. With this method, the dependent variables n_d, u_d, and ϕ are expanded in terms of their equilibrium and perturbed parts as $n_d = 1 + \tilde{n}_d$, $u_d = 0 + \tilde{u}_d$, and $\phi = 0 + \tilde{\phi}$. The perturbed quantities are proportional to $\exp[i(kx - \omega t)]$, and then the basic equations (1)–(5) are linearized and their corresponding first-order approximation yields

$$\tilde{n}_d = \frac{qk^2}{\omega\left(\omega + i\eta_d k^2\right)}\,\tilde{\phi}, \tag{6a}$$

$$\tilde{u}_d = \frac{qk}{\omega + i\eta_d k^2}\,\tilde{\phi}. \tag{6b}$$

From Poisson's equation (3), the linear dispersion relation follows

$$\left[k^2 + \mu_i\left(1-\beta\right) + \mu_e\sigma_i\right]\omega^2 + \\ + i\eta_d k^2\left[k^2 + \mu_i\left(1-\beta\right) + \mu_e\sigma_i\right]\omega - q^2k^2 = 0. \tag{7}$$

We set consider

$$\omega = \omega_r + i\omega_i, \tag{8}$$

where ω_r and ω_i are the real and imaginary parts of the plasma frequency ω. Inserting Eq. (8) into Eq. (7), we obtain

$$2\left(k^2 + \mu_i\left(1-\beta\right) + \mu_e\sigma_i\right)\omega_r\omega_i + \\ + \eta_d k^2\left(k^2 + \mu_i\left(1-\beta\right) + \mu_e\sigma_i\right)\omega_r = 0, \tag{9a}$$

$$\left(k^2 + \mu_i\left(1-\beta\right) + \mu_e\sigma_i\right)\omega_i^2 - \\ - \left(k^2 + \mu_i\left(1-\beta\right) + \mu_e\sigma_i\right)\omega_r^2 + \\ + \eta_d k^2\left(k^2 + \mu_i\left(1-\beta\right) + \mu_e\sigma_i\right)\omega_i + q^2k^2 = 0. \tag{9b}$$

Solving Eqs. (9), we obtain $\omega_r = 0$ and

$$\omega_i = \frac{-k^2\eta_d}{2} + \\ + \frac{\sqrt{-4q^2k^2 + k^4\eta_d^2\left(k^2 + \mu_i\left(1-\beta\right) + \mu_e\sigma_i\right)}}{2\sqrt{k^2 + \mu_i\left(1-\beta\right) + \mu_e\sigma_i}}, \tag{10}$$

which depends mainly on the plasma parameters k, η_d, σ_i, and α. The behavior of the damping rate ω_i with such parameters is illustrated in Figs. 1 and 2. From these figures, we can see that the instability damping rate ω_i increases as the plasma parameters (the carrier wave number k, the dust kinematic viscosity coefficient η_d, and the ion-to-electron temperature ratio σ_i) increase, and decreases as the nonthermal parameter α increases.

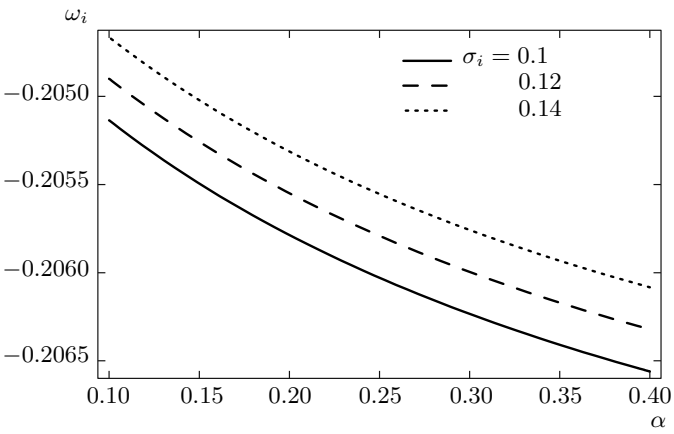

Fig. 1. The variation of ω_i versus α and σ_i for $\mu_e = 1.4$, $\mu_i = 0.4$, $\eta_d = 0.2$, $k = 5$, $q = 1$

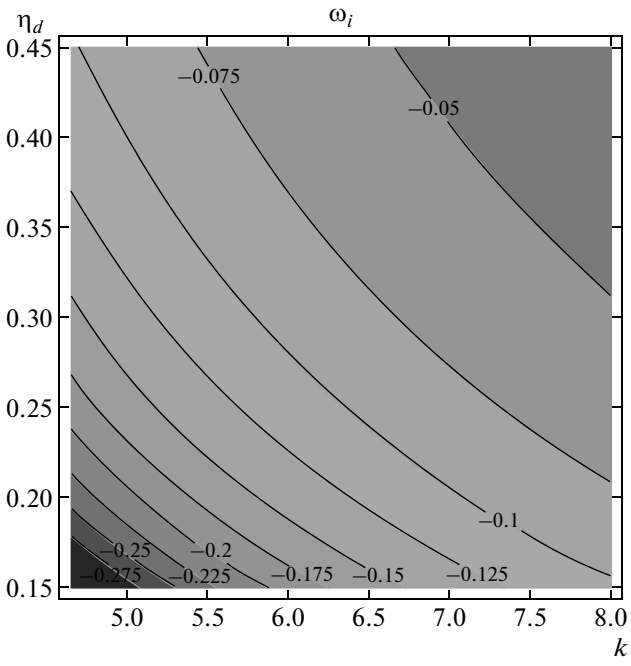

Fig. 2. Contour plot of ω_i versus η_d and k for $\mu_e = 1.1$, $\mu_i = 0.1$, $\alpha = 0.2$, $\sigma_i = 0.2$, $q = 1$

4. NONLINEAR ANALYSIS

To derive a dynamical equation for the nonlinear propagation of electrostatic waves in our plasma system, we use the reductive perturbation method. The reductive perturbation method should be applied to small-amplitude nonlinear waves [30]. This method rescales both space and time in the governing equations of the system so as to introduce space and time variables that are appropriate for the description of long-wavelength phenomena. According to this method, the independent variables are stretched as

$$\tau = \varepsilon^{3/2}t, \quad \xi = \varepsilon^{1/2}(x - \lambda t), \quad \eta_d = \varepsilon^{1/2}\,\eta, \tag{11}$$

where ε is a small dimensionless expansion parameter measuring the strength of the nonlinearity and λ is the wave speed. All physical quantities appearing in the basic equations (1)–(5) are expanded in power series in ε about their equilibrium values as

$$n_d = 1 + \varepsilon n_{d1} + \varepsilon^2 n_{d2} + \varepsilon^3 n_{d3} + \dots, \tag{12a}$$

$$u_d = \varepsilon u_{d1} + \varepsilon^2 u_{d2} + \varepsilon^3 u_{d3} + \dots, \tag{12b}$$

$$\phi = \varepsilon\phi_1 + \varepsilon^2\phi_2 + \varepsilon^3\phi_3 + \dots \tag{12c}$$

We substitute Eqs. (11) and (12) in the basic equations (1)–(5) and equate the corresponding coefficients of like powers of ε. From the lowest-order equations in ε, we then have

$$n_{d1} = \frac{q}{\lambda^2}\phi_1, \tag{13}$$

$$u_{d1} = \frac{q}{\lambda}\phi_1, \tag{14}$$

and Poisson's equation gives the compatibility condition

$$\lambda^2 = \frac{q^2}{\mu_e\sigma_i - \mu_i(\beta - 1)}. \tag{15}$$

Proceeding to the order ε^2, we obtain

$$\frac{\partial n_{d1}}{\partial\tau} - \lambda\frac{\partial n_{d2}}{\partial\xi} + \frac{\partial u_{d2}}{\partial\xi} + \frac{\partial\left(n_{d1}u_{d1}\right)}{\partial\xi} = 0, \tag{16a}$$

$$\frac{\partial u_{d1}}{\partial\tau} - \lambda\frac{\partial u_{d2}}{\partial\xi} + u_{d1}\frac{\partial u_{d1}}{\partial\xi} + q\frac{\partial\phi_2}{\partial\xi} - \eta\frac{\partial^2 u_{d1}}{\partial\xi^2} = 0, \tag{16b}$$

$$\frac{\partial^3\phi_1}{\partial\xi^3} + q\frac{\partial n_{d2}}{\partial\xi} - \frac{q^2}{\lambda^2}\frac{\partial\phi_2}{\partial\xi} + (\mu_i - \mu_e\sigma_i^2)\phi_1\frac{\partial\phi_1}{\partial\xi} = 0. \tag{16c}$$

Eliminating the second-order perturbed quantities n_{d2}, u_{d2}, and ϕ_2 and solving this system with the aid of Eqs. (13)–(15), we finally obtain the KdV–Burgers equation

$$\frac{\partial\phi_1}{\partial\tau} + A\,\phi_1\frac{\partial\phi_1}{\partial\xi} + B\,\frac{\partial^3\phi_1}{\partial\xi^3} + C\,\frac{\partial^2\phi_1}{\partial\xi^2} = 0, \tag{17}$$

where

$$A = \frac{3q}{2\lambda} + \frac{\lambda^3}{2q^2}(\mu_i - \mu_e\sigma_i^2), \tag{18a}$$

$$B = \frac{\lambda^3}{2q^2}, \quad C = -\frac{\eta}{2}. \tag{18b}$$

4.1. Bifurcation analysis and solutions of the KdV–Burgers equation

We introduce the variable $\chi = \xi - U\tau$, where χ is the transformed coordinate relative to a frame that moves with the velocity U. Integrating Eq. (17) with respect to χ leads to

$$\frac{d^2\phi_1}{d\chi^2} + \frac{C}{B}\frac{d\phi_1}{d\chi} + \frac{A}{2B}\phi_1^2 - \frac{U}{B}\phi_1 = 0. \tag{19}$$

Owing to the presence of the Burgers term

$$\frac{C}{B}\frac{d\phi_1}{d\chi},$$

Eq. (19) describes homogeneous and dissipative dusty plasmas. Hence, the phase paths of such equation are, in general, no longer level curves of the energy

$$H\left(\phi_1, \frac{d\phi_1}{d\chi}\right).$$

In the dissipative case, it is therefore reasonable to deal with $dH/d\chi$ rather than H. The KdV–Burgers equation (19) can be written in the general form

$$\frac{d^2\phi_1}{d\chi^2} + h\left(\phi_1, \frac{d\phi_1}{d\chi}\right)\frac{d\phi_1}{d\chi} + G(\phi_1) = 0, \tag{20}$$

where h and G are two functions that can be determined by comparing Eqs. (19) and (20).

In the conservative case ($h = 0$), the total energy associated with Eq. (20) is

$$H = \frac{1}{2}\left(\frac{d\phi_1}{d\chi}\right)^2 + V(\phi_1), \tag{21}$$

where $V(\phi_1)$ is the potential function; then

$$\frac{dH}{d\chi} = \frac{d\phi_1}{d\chi}\left(\frac{d^2\phi_1}{d\chi^2} + \frac{dV}{d\phi_1}\right). \tag{22}$$

With $G(\phi_1) = dV/d\phi_1$ in Eq. (20), the total derivative of H is given by

$$\frac{dH}{d\chi} = -h\left(\phi_1, \frac{d\phi_1}{d\chi}\right)\left(\frac{d\phi_1}{d\chi}\right)^2, \tag{23}$$

which is a decreasing function of χ if $h > 0$. This equation is very important for studying the stability of the system. In our case, $dH/d\chi$ corresponds to the KdV–Burgers equation:

$$\frac{dH}{d\chi} = \frac{C}{B}\left(\frac{d\phi_1}{d\chi}\right)^2, \tag{24}$$

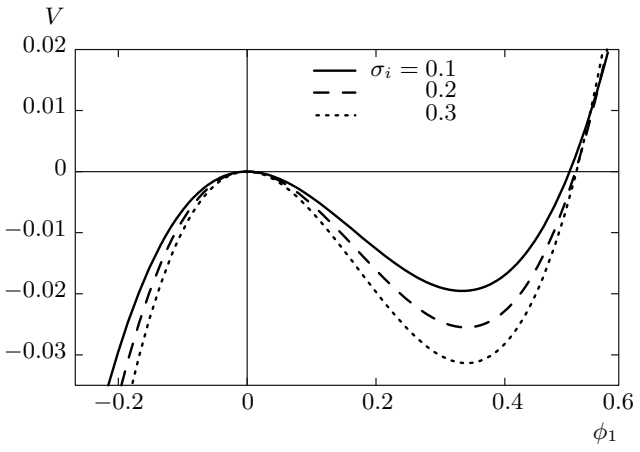

Fig. 3. The variation of V versus ϕ_1 at different values of σ_i for $\mu_e = 3$, $\mu_i = 2$, $\alpha = 0.2$, $u_0 = 0.4$, $q = 1$

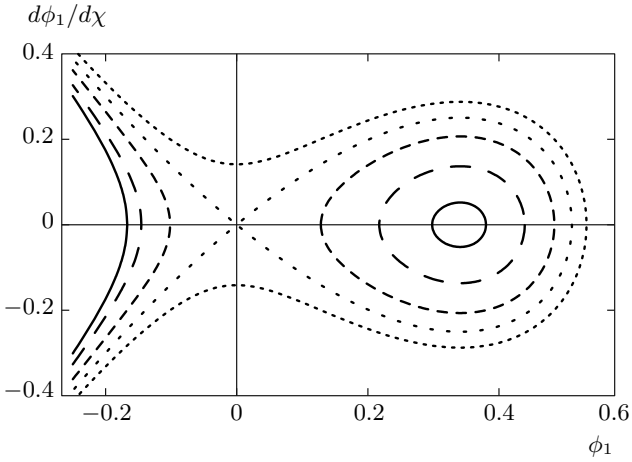

Fig. 4. The variation of $d\phi_1/d\chi$ versus ϕ_1 at different values of H for $\mu_e = 3$, $\mu_i = 2$, $\alpha = 0.2$, $\sigma_i = 0.3$, $u_0 = 0.4$, $q = 1$

which shows that the energy of the plasma system is not conserved and hence it is not easy to find an exact analytic solution of the KdV–Burgers equation.

In terms of the viscosity coefficient η, Eq. (24) can be written as

$$\frac{dH}{d\chi} = -\frac{q^2\eta}{\lambda^3}\left(\frac{d\phi_1}{d\chi}\right)^2, \tag{25}$$

which is always a decreasing function because q^2, η, and λ are always positive quantities.

In particular, if the Burgers coefficient $C = 0$, the system of equations becomes conservative ($dH/d\chi = 0$) and the total energy is

$$H = \frac{1}{2}\left(\frac{d\phi_1}{d\chi}\right)^2 - \frac{U}{2B}\phi_1^2 + \frac{A}{6B}\phi_1^3, \tag{26}$$

where the potential function is

$$V(\phi_1) = -\frac{U}{2B}\phi_1^2 + \frac{A}{6B}\phi_1^3. \tag{27}$$

Equations (26) and (27) are necessary to furnish the bifurcation and the phase portrait associated with this type of the KdV–Burgers equation. The profile of the potential function and the phase portrait are investigated under the conditions $A > 0$, $B > 0$, and $U > 0$; they are shown graphically in Figs. 3 and 4. The potential function is shown as a function of ϕ_1 for different values of σ_i in Fig. 3. It is clear that the potential well has one hump and a pit and the potential well becomes deeper as σ_i increases. The hump corresponds to a saddle point at $(0, 0)$ and the pit corresponds to the central point at $(2U/A,\ 0)$ in the phase portrait. From the topology of the phase portrait diagram in Fig. 4, we can see a family of periodic orbits at $(2U/A,\ 0)$, which predict a family of periodic wave solutions, and one homoclinic orbit at $(0, 0)$, that relates to one solitary wave solution. Moreover, Fig. 4 shows a series of bounded open orbits that correspond to a series of breaking wave solutions.

The trajectories shown in Fig. 4 point to the existence of a stable solitonic solution that should satisfy the condition

$$\left[\frac{d^2V}{d\phi_1^2}\right]_{\phi_1=0} < 0,$$

which explains that there must exist a nonzero crossing point $\phi_1 = \phi_0$ such that $V(\phi_1 = \phi_0) = 0$. In addition, there must exist a ϕ_1 between $\phi_1 = 0$ and $\phi_1 = \phi_0$ such that $V(\phi_1) < 0$. Obviously, it follows from Eq. (27) that the condition of the existence of a stable solitonic solution is satisfied because

$$\left[\frac{d^2V}{d\phi_1^2}\right]_{\phi_1=0} = -\frac{U}{B} < 0, \tag{28}$$

where the parameters U and B are positive. The corresponding stable solitonic solution is given by

$$\phi_1 = \phi_0\,\mathrm{sech}^2\left(\frac{\chi}{W}\right), \tag{29}$$

where $\phi_0 = 3U/A$ is the soliton wave amplitude and $W = \sqrt{4B/U}$ is the width of the soliton wave in the absence of the Burgers term. The behavior of the obtained solution and its amplitude and width are presented in Figs. 5–9. Figures 5 and 6 show the variation in ϕ_1 with χ at different values of α (the nonthermal

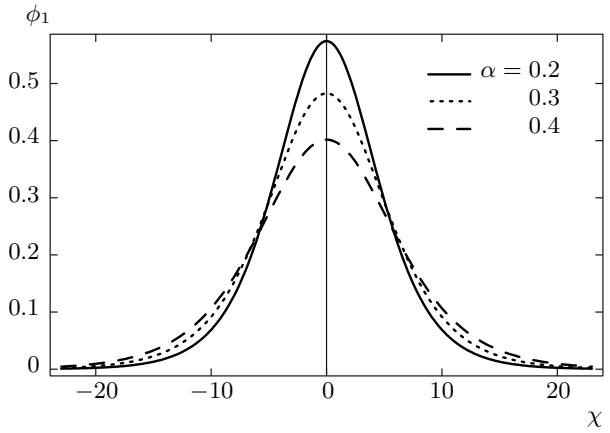

Fig. 5. The variation of ϕ_1 versus χ at different values of α for $\mu_e = 1.4$, $\mu_i = 0.4$, $\sigma_i = 0.2$, $u_0 = 0.4$, $q = 1$

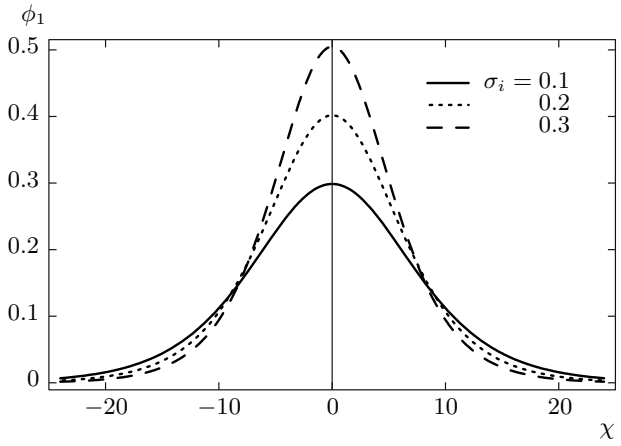

Fig. 6. The variation of ϕ_1 versus χ at different values of σ_i for $\mu_e = 1.4$, $\mu_i = 0.4$, $\alpha = 0.4$, $u_0 = 0.4$, $q = 1$

parameter) and σ_i (the ratio of the ion temperature to the electron temperature). The amplitude of the soliton wave decreases (increases) with increasing of α (σ_i), while the width increases (decreases) with increasing α (σ_i). The single-pulse soliton solution ϕ_1 is plotted versus ξ, and its propagation is shown at different time scales τ in Fig. 7. Both the amplitude and the width of the soliton waves are plotted against α and σ_i in Figs. 8 and 9, and the same behavior as in Figs. 5 and 6 is observed.

The soliton energy E_n is obtained as the integral

$$E_n = \int_{-\infty}^{\infty} u_{d1}^2(\chi)\, d\chi. \qquad (30)$$

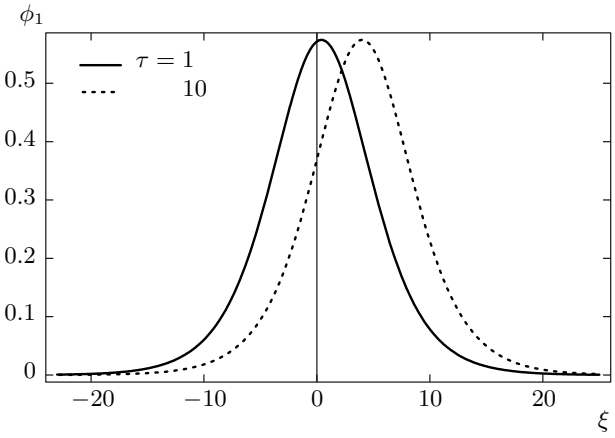

Fig. 7. The variation of ϕ_1 versus ξ at different values of τ for $\mu_e = 1.4$, $\mu_i = 0.4$, $\alpha = 0.2$, $\sigma_i = 0.2$, $u_0 = 0.4$, $q = 1$

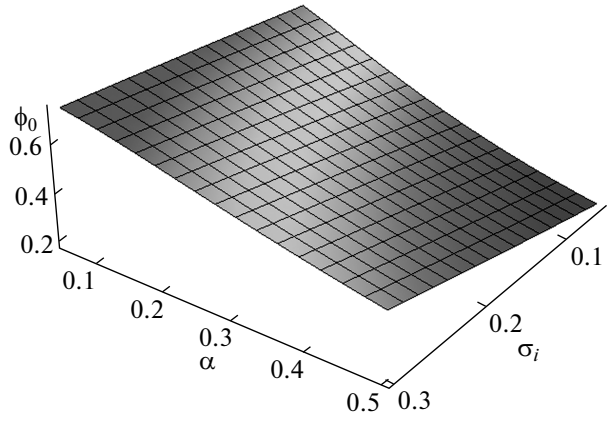

Fig. 8. The variation of ϕ_0 versus α and σ_i for $\mu_e = 1.4$, $\mu_i = 0.4$, $u_0 = 0.4$, $q = 1$

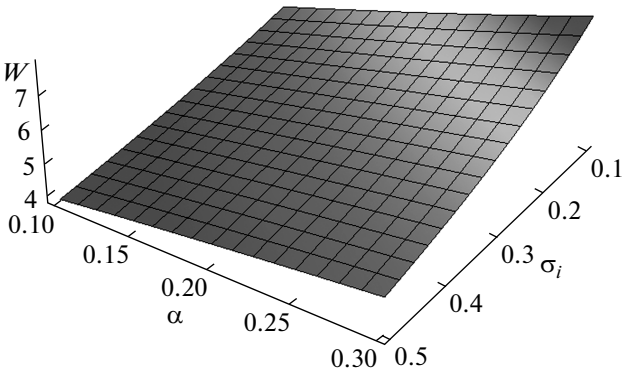

Fig. 9. The variation of W versus α and σ_i for $\mu_e = 1.4$, $\mu_i = 0.4$, $u_0 = 0.4$, $q = 1$

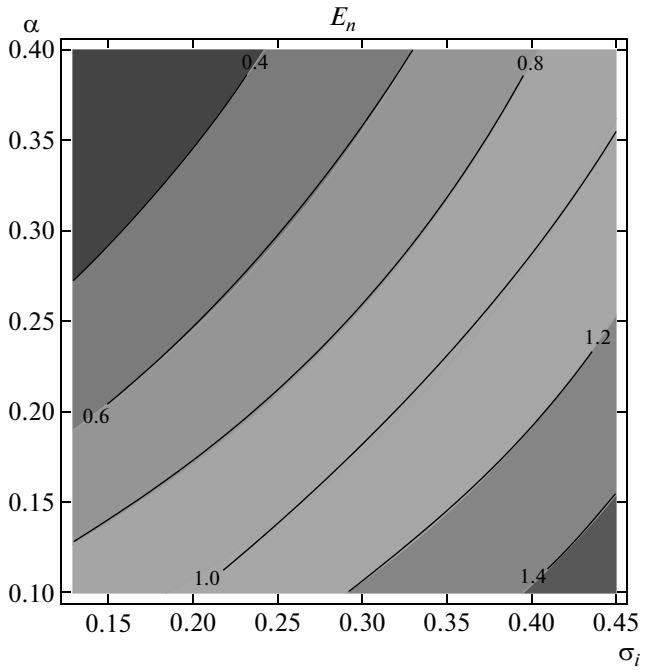

Fig. 10. Contour plot of E_n versus α and σ_i for $\mu_e = 1.4$, $\mu_i = 0.4$, $u_0 = 0.4$, $q = 1$

With Eqs. (14) and (29), Eq. (30) is readily integrated and yields the soliton energy

$$E_n = \frac{24q^2U^2}{\lambda^2 A^2\sqrt{U/B}}. \tag{31}$$

It is clear that the soliton energy depends mainly on the plasma parameters via the coefficients A and B. The behavior of the soliton energy as a function of α and σ_i is shown graphically in Fig. 10. We see from this figure that the soliton energy E_n increases (decreases) with increasing the value of σ_i (α).

The associated electric field is obtained as

$$\mathbf{E} = -\nabla\phi_1, \tag{32}$$

which gives

$$E = \frac{3U\sqrt{U/B}}{A}\operatorname{sech}^2\left(\frac{1}{2}\sqrt{\frac{U}{B}}\chi\right) \times \times \tanh\left(\frac{1}{2}\sqrt{\frac{U}{B}}\chi\right). \tag{33}$$

The behavior of the electric field E is presented graphically in Figs. 11–13. Figures 11 and 12 show the variation of the electric field E as a function of α and σ_i. Obviously, the amplitude of the electric field decreases

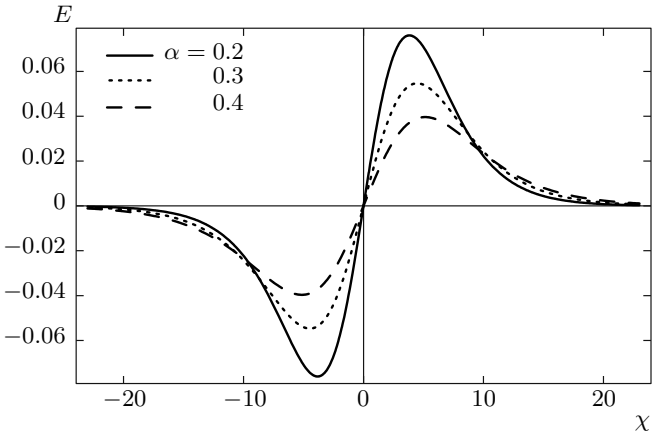

Fig. 11. The variation of E versus χ at different values of α for $\mu_e = 1.4$, $\mu_i = 0.4$, $\sigma_i = 0.2$, $u_0 = 0.4$, $q = 1$

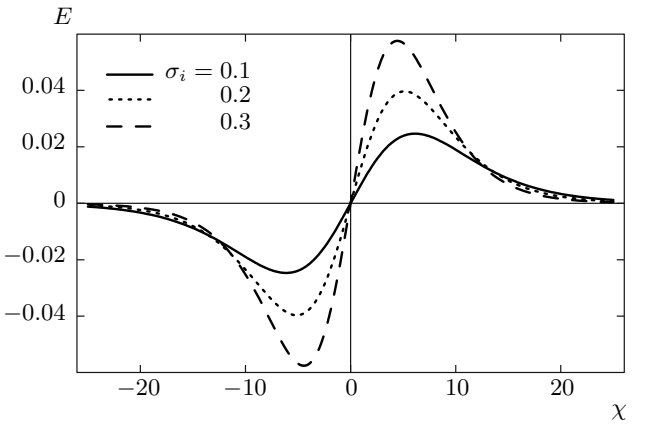

Fig. 12. The variation of E versus χ at different values of σ_i for $\mu_e = 1.4$, $\mu_i = 0.4$, $\alpha = 0.4$, $u_0 = 0.4$, $q = 1$

(increases) with increasing the value of α (σ_i), while the width of the electric field increases (decreases) with increasing the value of α (σ_i). Figure 13 represents the evolution of the electric field E versus ξ at different time scales τ.

In the presence of the Burgers term, the system of equations is dissipative and the total energy H is not conservative. Therefore, the exact solution of Eq. (19) can be constructed by means of different mathematical methods [29, 40–42]. Among these, the tanh method has proved to be a powerful mathematical technique for solving nonlinear differential equations.

Following the procedure of the tanh method [43], we consider the solution in the series form as

$$\phi_1 = \sum_{n=0}^{N} a_n \tanh^n(\chi), \tag{34}$$

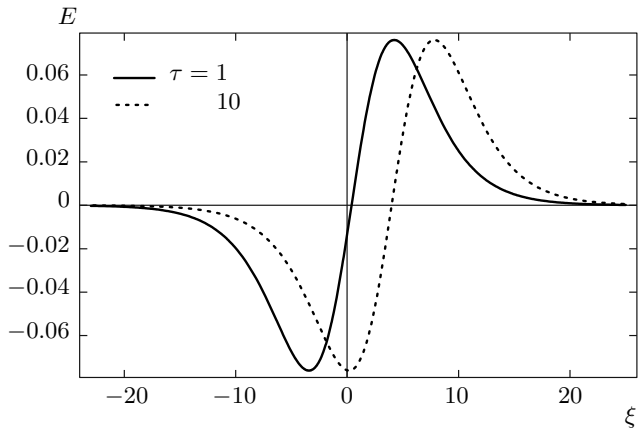

Fig. 13. The variation of E versus ξ at different values of τ for $\mu_e = 1.4$, $\mu_i = 0.4$, $\alpha = 0.2$, $\sigma_i = 0.2$, $u_0 = 0.4$, $q = 1$

where the coefficients a_n and N are to be determined. Balancing the nonlinear and dispersion terms in Eq. (19), we obtain $N = 2$. Substituting Eq. (34) in Eq. (19) and equating the different coefficients of different powers of $\tanh(\chi)$ functions to zero, we obtain the set of algebraic equations

$$2a_2 - \frac{U}{B}a_0 + \frac{A}{2B}a_0^2 + \frac{C}{B}a_1 = 0, \tag{35a}$$

$$2a_1 + \frac{U}{B}a_1 - \frac{A}{B}a_0a_1 - \frac{2C}{B}a_2 = 0, \tag{35b}$$

$$8a_2 + \frac{U}{B}a_2 - \frac{A}{2B}a_1^2 - \frac{A}{B}a_0a_2 + \frac{C}{B}a_1 = 0, \tag{35c}$$

$$2a_1 + \frac{A}{B}a_1a_2 - \frac{2C}{B}a_2 = 0, \tag{35d}$$

$$6a_2 + \frac{A}{2B}a_2^2 = 0. \tag{35e}$$

Solving these algebraic equations, we obtain

$$a_0 = \frac{U}{B} + \frac{8B}{A} + \frac{C^2}{25AB}, \tag{36a}$$

$$a_1 = \frac{12C}{5A}, \quad a_2 = \frac{-12B}{A}, \tag{36b}$$

$$C = -10B, \quad U = 24B. \tag{36c}$$

Hence, we can write the explicit solution of KdV–Burgers equation (19) as

$$\phi_1 = \frac{1}{A}\left(U + 8B + \frac{C^2}{25B} + \frac{12C}{5}\tanh(\chi) - 12B\tanh^2(\chi)\right), \tag{37}$$

or

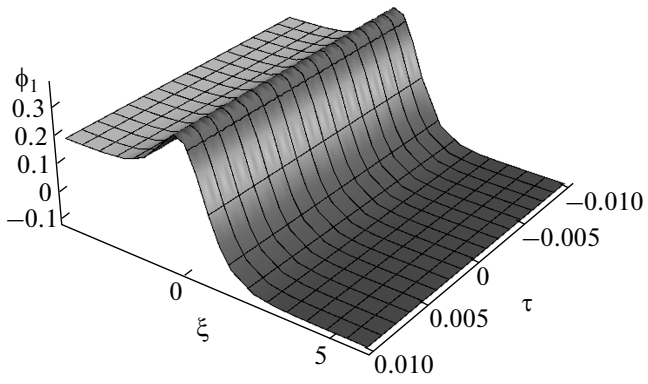

Fig. 14. The evolution of ϕ_1 versus ξ and τ for $\mu_e = 6$, $\mu_i = 5$, $\alpha = 0.2$, $\sigma_i = 0.2$, $\eta = 0.4$, $u_0 = 0.4$, $q = 1$

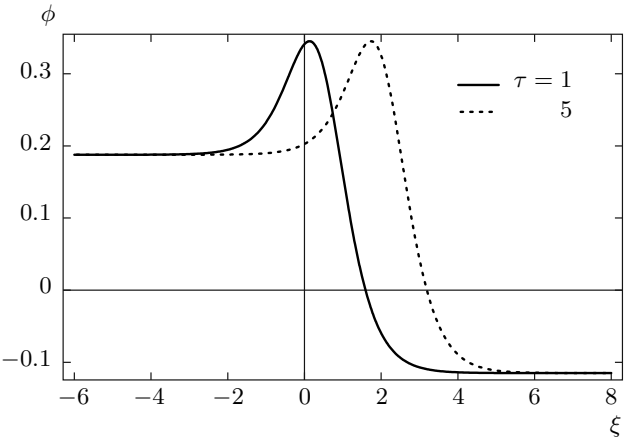

Fig. 15. The variation of ϕ_1 versus ξ at different values of τ for $\mu_e = 6$, $\mu_i = 5$, $\alpha = 0.2$, $\sigma_i = 0.2$, $\eta = 0.4$, $u_0 = 0.4$, $q = 1$

$$\phi_1 = \frac{1}{A}\left(U - 4B + \frac{C^2}{25B} + \frac{12C}{5}\tanh(\chi) + 12B\,\mathrm{sech}^2(\chi)\right). \tag{38}$$

This class of solutions represents a particular combination of a solitary wave (the $\mathrm{sech}^2(\chi)$ term in the right-hand side of Eq. (38)) with a Burgers shock wave (the $\tanh(\chi)$ term). The behavior of this solution in terms of the coordinates ξ and τ is shown graphically in Figs. 14 and 15. We can see from these figures that both soliton and shock structures are obtained due to the presence of dispersive and dissipative coefficients.

Another type of solution can be obtained when the dissipative term is dominant over the dispersive term. In this case, Eq. (19) reduces to the nonlinear first-order differential equation

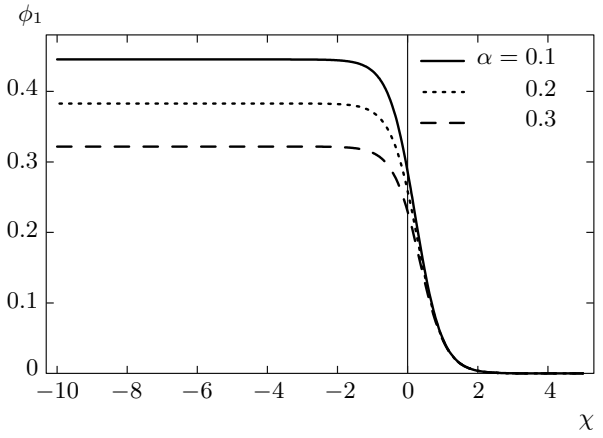

Fig. 16. The variation of ϕ_1 versus χ at different values of α for $\mu_e = 1.4$, $\mu_i = 0.4$, $\sigma_i = 0.2$, $\eta = 0.3$, $u_0 = 0.4$, $q = 1$

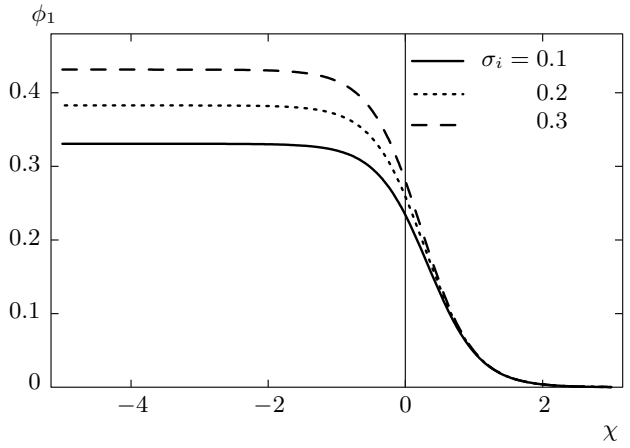

Fig. 17. The variation of ϕ_1 versus χ at different values of σ_i for $\mu_e = 1.4$, $\mu_i = 0.4$, $\alpha = 0.2$, $\eta = 0.3$, $u_0 = 0.4$, $q = 1$

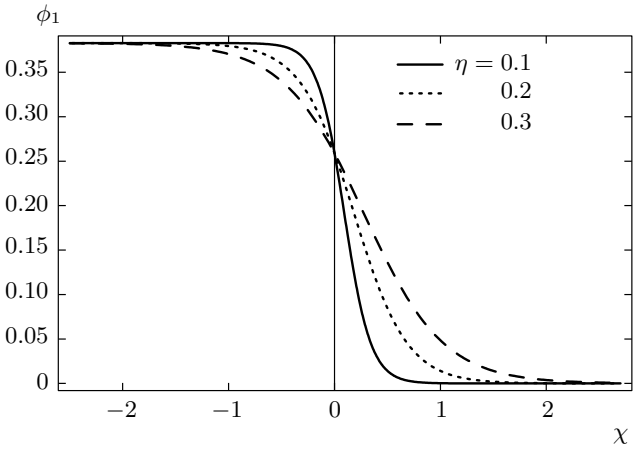

Fig. 18. The variation of ϕ_1 versus χ at different values of η for $\mu_e = 1.4$, $\mu_i = 0.4$, $\alpha = 0.2$, $\sigma_i = 0.2$, $u_0 = 0.4$, $q = 1$

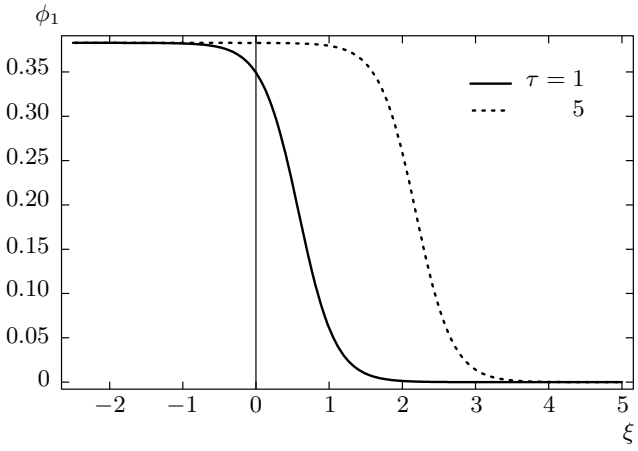

Fig. 19. The variation of ϕ_1 versus ξ at different values of τ for $\mu_e = 1.4$, $\mu_i = 0.4$, $\alpha = 0.2$, $\sigma_i = 0.2$, $\eta = 0.2$, $u_0 = 0.4$, $q = 1$

$$\frac{d\phi_1}{d\chi} = \frac{U}{C}\phi_1 - \frac{A}{2C}\phi_1^2, \tag{39}$$

which admits the solution

$$\phi_1 = \frac{2U\exp\left(U\chi/C\right)}{1 + A\exp\left(U\chi/C\right)}, \tag{40}$$

or

$$\phi_1 = \frac{U}{A}\left[1 + \tanh\left(\frac{U}{2C}\chi\right)\right]. \tag{41}$$

This type of solution actually describes a monotonic shock wave, whose behavior is shown in Figs. 16–19. These figures investigate the effect of plasma parameters like α, σ_i, and the dust kinematic viscosity coefficient η on the existence of monotonic shocks. Figures 16 and 17 indicate that the monotonic shock wave strength decreases (increases) with increasing the value of α (σ_i). However, in Fig. 18, the monotonic shock wave width increases with increasing the value of η. The propagation of a monotonic shock wave at different time scales is shown in Fig. 19.

On the other hand, another type of solution of special interest can be obtained if we consider the asymptotic boundary condition

$$\chi \to \pm\infty \Rightarrow \frac{d^2\phi_1}{d\chi^2} = \frac{d\phi_1}{d\chi} = 0,$$

which yields the asymptotic solution of the nonlinear KdV–Burgers differential equation as

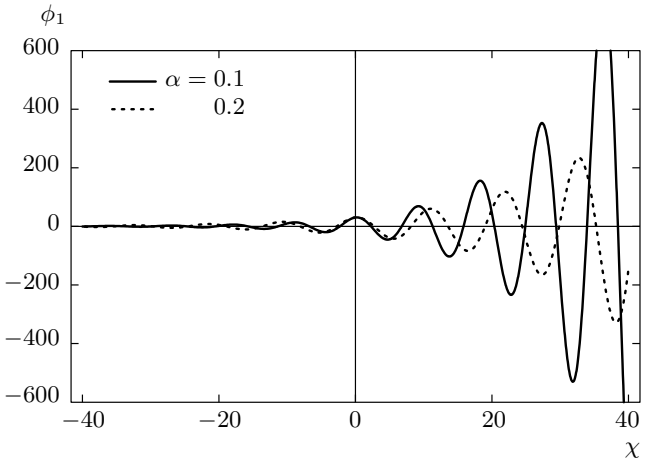

Fig. 20. The variation of ϕ_1 versus χ at different values of α for $\mu_e = 1.8$, $\mu_i = 0.8$, $\sigma_i = 0.2$, $\eta = 0.3$, $u_0 = 0.4$, $q = 1$

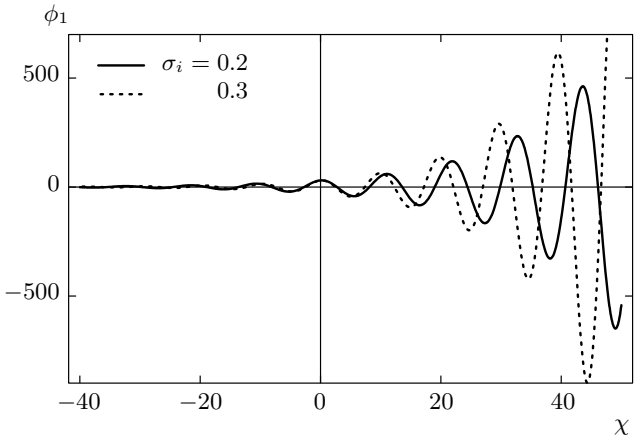

Fig. 21. The variation of ϕ_1 versus χ at different values of σ_i for $\mu_e = 1.8$, $\mu_i = 0.8$, $\alpha = 0.2$, $\eta = 0.3$, $u_0 = 0.4$, $q = 1$

$$\phi_c = \frac{2U}{A}. \tag{42}$$

Using that $\phi_1 = \phi_c + \Phi$ for $|\phi_c| \gg |\Phi|$, Eq. (19) can be linearized to the second-order linear differential equation

$$\frac{d^2\Phi}{d\chi^2} + \frac{C}{B}\frac{d\Phi}{d\chi} + \frac{U}{B}\Phi = 0. \tag{43}$$

The solution of linear differential equation (43) can be expressed in the exponential form $\Phi = \exp(M\chi)$, where

$$M = \frac{C}{2B}\left[-1 \pm \sqrt{1 - \frac{4UB}{C^2}}\right]. \tag{44}$$

For $C^2 \ll 4UB$, the oscillatory shock wave solution is given by

$$\phi_1 = \phi_c + Q\exp\left(-\frac{C}{2B}\chi\right)\cos\left(\sqrt{\frac{U}{B}}\chi\right). \tag{45}$$

where Q is an arbitrary constant. The behavior of the obtained solution with the parameters α, σ_i, and η is shown graphically in Figs. 20–22. These figures show that the amplitude of the oscillatory shock wave decreases with increasing the value of α and increases with increasing the values of both σ_i and η.

Obviously, in addition to an oscillatory shock wave, the KdV–Burgers equation exhibits solitonic and monotonic shock waves due to the Burgers term arising from the fluid viscosity.

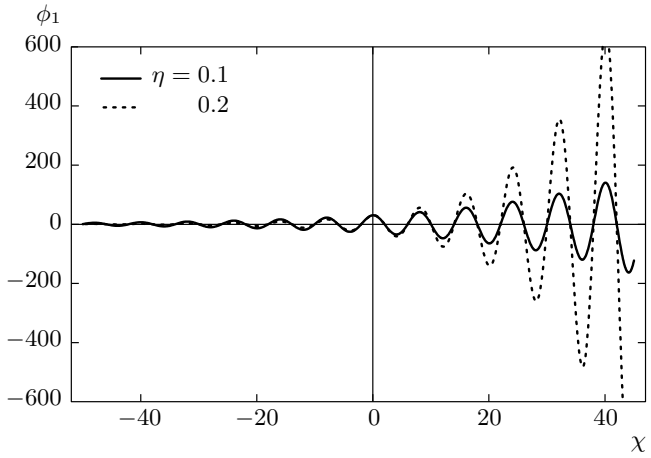

Fig. 22. The variation of ϕ_1 versus χ at different values of η for $\mu_e = 2.2$, $\mu_i = 1.2$, $\alpha = 0.2$, $\sigma_i = 0.2$, $u_0 = 0.4$, $q = 1$

5. CONCLUSION

The present investigation describes the formation and basic properties of linear and nonlinear DA waves in a homogeneous system of an unmagnetized, collisionless and dissipative dusty space plasma whose constituents are negatively charged dust grains, nonthermal ions, and electrons obeying the Boltzmann thermal distribution. In the linear analysis, the normal mode method is used to reduce the basic set of fluid equations to a linear dispersion relation. An expression for the damping rate ω_i is obtained and its behavior with the plasma parameters is plotted in Figs. 1 and 2. These plots show that the damping rate increases as

the carrier wave number k, the kinematic dust viscosity coefficient η_d, and the ratio of the ion temperature to the electron temperature σ_i increase, while it decreases as the nonthermal parameter α increases. In the nonlinear analysis, the reductive perturbation technique has been used to derive the KdV–Burgers equation, which is not an integrable Hamiltonian system. This means that the energy of the plasma system is not conserved due to the Burgers dissipation term.

In the absence of the Burgers term ($C = 0$), the bifurcation and the phase portrait associated with this type of the KdV–Burgers equation are investigated graphically in Figs. 3 and 4, under the conditions $A > 0$, $B > 0$, and $U > 0$. The topology of the phase portrait and potential diagram refer to wide classes of traveling wave solutions. One of these solutions is related to soliton solution (29), which is obtained when the dissipation effect is negligible in comparison with that of the nonlinearity and dispersion. The behavior of such a solution is shown graphically in Figs. 5–9, which indicate that the amplitude of the soliton wave decreases (increases) with increasing $\alpha(\sigma_i)$, but the width increases (decreases) with increasing α (σ_i). Also, the energy of the soliton wave is calculated and plotted in Fig. 10. It is observed that the soliton energy E_n increases (decreases) with increasing the value of σ_i (α). The electric field associated with the potential function ϕ_1, Eq. (29), is also plotted with the wave variable χ, Figs. 11–13. Clearly, the amplitude of the electric field decreases (increases) with increasing the value of α (σ_i), while its width increases (decreases) with increasing the value of α (σ_i).

In the presence of the Burgers term, $C \neq 0$, the KdV–Burgers equation admits three classes of analytic solutions of physical interest. But these solutions are related to a combination of shock and soliton waves, monotonic and oscillatory shocks. A combination of shock and soliton waves is obtained explicitly by using the tanh method, and its behavior is shown in Figs. 14 and 15. The monotonic shock wave can also exist when the dissipation term is dominant over the dispersive term and its behavior is shown in Figs. 16–19. These figures indicate that the monotonic shock wave strength decreases (increases) with increasing the value of α (σ_i), while its width increases with increasing the value of η. The oscillatory shock wave can exist when the dispersive term is dominant over the dissipative term. Figures 20–22 show that the amplitude of such a wave decreases with increasing the value of α and increases with increasing the values of both σ_i and η. Finally, we conclude that the Burgers term due to fluid viscosity plays an essential role in formation of soliton, monotonic, and oscillatory shock waves in plasmas. The present study has contributed to a better understanding of the propagation characteristics of the DA waves, which are of vital importance in laboratory plasma and as in space plasma.

The nonideality effects such as viscosity, turbulence, particle reflection, Landau damping and charge fluctuations cause dissipation and then the shock waves structure may be generated. The effect of other interactions can be investigated in our future work taking the nonuniform distribution of the dust density into account.

The authors thank the referee for their efforts and valuable remarks.

REFERENCES

1. C. K. Goertz, Rev. Geophys. **27**, 271 (1989).
2. T. G. Northrop, Phys. Scripta **45**, 475 (1992).
3. D. A. Mendis and M. Rosenberg, Ann. Rev. Astron. Astrophys. **32**, 419 (1994).
4. F. Verheest, Space Sci. Rev. **77**, 267 (1996).
5. B. Feuerbacher, R. T. Willis, and B. Fitton, Astrophys. J. **181**, 101 (1973).
6. H. Fechting, E. Grün, and G. E. Morfill, Planet. Space Sci. **27**, 511 (1979).
7. O. Havnes, C. K. Goertz, G. E. Morfill, E. Grün, and W. Ip, J. Geophys. Res. **92**, 2281 (1987).
8. N. N. Rao, P. K. Shukla, and M. Y. Yu, Planet. Space Sci. **38**, 543 (1990).
9. A. Barkan, R. L. Merlino, and N. D'Angelo, Phys. Plasmas **2**, 3563 (1995).
10. P. K. Shukla and V. P. Silin, Phys. Scripta **45**, 508 (1992).
11. P. K. Shukla and H. U. Rahman, Planet. Space Sci. **46**, 541 (1998).
12. P. K. Shukla, M. Yu, and Y. R. Bharuthram, J. Geophys. Res. **96**(21), 343 (1991).
13. B. Farokhi and M. Shahmansouri, Phys. Scripta **79**, 065501 (2009).
14. M. Shahmansouri and B. Farokhi, J. Plasma Phys. **78**, 259 (2012).
15. R. A. Cairns, A. A. Mamun, R. Bingham, R. Dendy, R. Boström, C. M. C. Nairns, and P. K. Shukla, Geophys. Res. Lett. **22**, 2709 (1995).

16. J. R. Asbridge, S. J. Bame, and I. B. Strong, J. Geophys. Res. **73**, 5777 (1968).

17. L. P. Zhang and J. K. Xue, Chin. Phys. B **17**, 2594 (2008).

18. O. Ishihara, J. Phys. D **40**, R121 (2007).

19. P. K. Shukla and B. Eliasson, Rev. Mod. Phys. **81**, 23 (2009).

20. A. Saha and P. Chatterjee, Astrophys. Space Sci. **349**, 813 (2014).

21. A. A. Mamun, Astrophys. Space Sci. **268**, 443 (1999).

22. A. A. Mamun and P. K. Shukla, Phys. Plasmas **9**, 1468 (2002).

23. A. A. Mamun, Phys. Lett. A **372**, 884 (2008).

24. A. A. Mamun and R. A. Cairns, Phys. Rev. E **79**, 05540(R) (2009).

25. P. Bandyopadhyay, G. Prasad, A. Sen, and P. K. Kaw, Phys. Lett. A **368**, 491 (2007).

26. R. Heidemann, S. Zhdanov, R. Sütterlin, H. M. Thomas, and G. E. Morfill, Phys. Rev. Lett. **102**, 135002 (2009).

27. W. S. Duan, Chaos, Solitons, and Fractals **14**, 503 (2002).

28. S. K. El-Labany, W. M. Moslem, and F. M. Safy, Phys. Plasmas **13**, 082903 (2006).

29. S. A. El-Wakil, A. M. El-Hanbaly, E. K. El-Shewy, and I. E. El-Kamash, J. Theor. Appl. Phys. **8**, 130 (2014).

30. T. Taniuti and N. Yajima, J. Math. Phys. **10**, 1369 (1969).

31. S. V. Singh and N. N. Rao, J. Plasma Phys. **60**, 541 (1998).

32. S. I. Popel, A. A. Gisko, A. P. Golub, T. V. Losseva, R. Bingham, and P. K. Shukla, Phys. Plasmas **7**, 2410 (2000).

33. Y. Nakamura and A. Sarma, Phys. Plasmas **8**, 3921 (2001).

34. L. P. Zhang and J. K. Xue, Phys. Plasmas **12**, 042304 (2005).

35. K. B. Zhang and H. Y. Wang, J. Korean Phys. Soc. **55**, 1461 (2009).

36. Z. J. Zhou, H. Y. Wang, and K. B. Zhang, Pramana **78**, 127 (2011).

37. M. Shahmansouri, Iran. J. Sci. Technol. **37**(A3), 285 (2013).

38. P. K. Shukla and A. A. Mamun, *Introduction to Dusty Plasma Physics*, CRC Press, Bristol (2002).

39. S. Sultan and I. Kourakis, Eur. Phys. J. D **66**, 100 (2012).

40. A. El-Hanbaly, J. Phys. A **36**, 8311 (2003).

41. A. El-Hanbaly and M. Abdou, J. Appl. Math. Comput. **182**, 301 (2006).

42. S. Mahmood and H. Ur-Rehman, Phys. Plasmas **17**, 072305 (2010).

43. W. Malfliet and W. Hereman, Phys. Scripta **54**, 563 (1996).